

Achieving the Tightest Relaxation of Sigmoids for Formal Verification

Samuel Chevalier¹, Duncan Starkenburg¹, Krishnamurthy (Dj) Dvijotham²

¹University of Vermont

²ServiceNow

samuel.chevalier@uvm.edu, duncan.starkenburg@uvm.edu, dvij@cs.washington.edu

Abstract

In the field of formal verification, Neural Networks (NNs) are typically reformulated into equivalent mathematical programs which are optimized over. To overcome the inherent non-convexity of these reformulations, convex relaxations of nonlinear activation functions are typically utilized. Common relaxations (i.e., static linear cuts) of “S-shaped” activation functions, however, can be overly loose, slowing down the overall verification process. In this paper, we derive tuneable hyperplanes which upper and lower bound the sigmoid activation function. When tuned in the dual space, these affine bounds smoothly rotate around the nonlinear manifold of the sigmoid activation function. This approach, termed α -sig, allows us to tractably incorporate the tightest possible, element-wise convex relaxation of the sigmoid activation function into a formal verification framework. We embed these relaxations inside of large verification tasks and compare their performance to LiRPA and α -CROWN, a state-of-the-art verification duo.

Introduction

Formal verification has an ever-widening spectrum of important uses, including mathematical proof validation (Trinh et al. 2024), adversarially robust classification (Zhang et al. 2022a), data-driven controller reachability analysis (Everett 2021), performance guarantees for surrogate models of the electric power grid (Chevalier and Chatzivasileiadis 2024), and more (Urban and Miné 2021). The formal verification of Neural Networks (NNs), in particular, has seen a flurry of recent research activity. Pushed by the international Verification of Neural Networks Competition (VNN-Comp), NN verification technologies have scaled rapidly in recent years (Brix et al. 2023b,a). Competitors have exploited, and synergistically spurred, the development of highly successful verification algorithms, e.g., α , β -CROWN (Wang et al. 2021; Lyu et al. 2019), Multi-Neuron Guided Branch-and-Bound (Ferrari et al. 2022), DeepPoly (Singh et al. 2019), etc. The winningest methods emerging from VNN-Comp serve as the leading bellwethers for state-of-the-art within the NN verification community.

Despite these advances, verification technologies cannot yet scale to Large Language Model (LLM) sized sys-

tems (Sun et al. 2024). Nonlinear, non-ReLU activation functions present one of the key computational obstacles which prevents scaling. While these activation functions can be attacked with spatial Branch-&-Bound (B&B) approaches (Shi et al. 2024), authors in (Wu et al. 2023) note that “existing verifiers cannot tightly approximate S-shaped activations.” The sigmoid activation is one such S-shaped activation function which is challenging to deal with. Given its close relationship to the ubiquitous softmax function (Wei et al. 2023), which is embedded in modern transformer layers (Ildiz et al. 2024), efficient verification over the sigmoid activation function would help boost verification speeds and generally help extend verification technology applicability.

Our contributions. Given the ongoing computational challenge of verifying over NNs containing sigmoid activation functions, our contributions follow:

1. We derive an explicit mapping between the linear slope and y-intercept point of a tangent line which tightly bounds a sigmoid. This differentiable, tunable mapping is embedded into a verification framework to yield the tightest possible element-wise relaxation of the sigmoid.
2. We propose a “backward” NN evaluation routine which dynamically detects if a sigmoid should be upper or lower bounded at each step of a gradient-based solve.
3. To ensure feasible projection in the dual space, we design a sequential quadratic program which efficiently pre-computes maximum slope bounds of all tunable slopes.

Many verification algorithms exploit element-wise convex relaxation of nonlinear activation functions, resulting in convex solution spaces (Salman et al. 2020). The stacking up of tightening dual variables within a dualized problem reformulation, as in α , β -CROWN, can lead to a formally *nonconvex* mathematical program. Similarly, the verification formulation which we present in this paper is nonconvex, but it globally lower bounds the true verification solution. Authors in (Bunel et al. 2020) have shown that spurious local minima in nonconvex problems containing “staged convexity” are very rare, and they even design perturbation-based approaches to avoid them. In this paper, we use a gradient-based approach to solve a formally nonconvex problem, but solutions smoothly converge to what appears to be a global maximum.

Related Works

To iteratively tighten relaxed ReLU-based NNs, the architects of α -CROWN (Xu et al. 2021) use the “optimizable” linear relaxation demonstrated in Fig. 1. In this approach, the parameter α is tuned to achieve a maximally tight lower bound on the verification problem. Authors in (Salman et al. 2020) showed α variables to be equivalent to the dual variables of an associated linear program (LP)-relaxed verification problem. (Wang et al. 2021) applied the α -CROWN approach within a B&B context, introducing new split-constraint dual variables β to be optimized over in the dual space. More recently, (Shi et al. 2024) developed a general framework (GenBaB) to perform B&B over a wide class of nonlinear activations, including sigmoid, tanh, sine, GeLU, and bilinear functions. The authors utilize pre-optimized branching points in order to choose linear cuts which statically bound portions of the activation functions. Critically, they also incorporate optimizable linear relaxations of the bilinear, sine, and GeLU activation functions using α -like tunable parameters.

Verification over “S-shaped” activation functions is considered in (Wu et al. 2023), where the authors use sequential identification of counterexamples in the relaxed search space to iteratively tighten the activation relaxations. Authors in (Zhang et al. 2022b) propose a verification routine which incorporates the provably tightest linear approximation of sigmoid-based NNs. Notably, the approach uses static (i.e., non-tunable) linear approximations, improving upon other works whose sigmoid relaxations minimize relaxation areas (Henriksen and Lomuscio 2020) or use parallel upper and lower bounding lines (Wu and Zhang 2021). While existing approaches have designed advanced cut selection procedures for sigmoid activation functions, and even embedded these procedures within B&B, there exists no explicitly optimizable, maximally tight linear relaxation strategy for sigmoid activation functions.

Formal Verification Framework

Let $x \in \mathbb{R}^{n_1}$ be the input to an L -layer NN mapping $\text{NN}(\cdot) : \mathbb{R}^{n_1} \rightarrow \mathbb{R}^{n_L}$. A scalar verification metric function, $m(\cdot) : \mathbb{R}^{n_L} \rightarrow \mathbb{R}^1$, wraps around the NN to generate the verification function $f(x) \triangleq m(\text{NN}(x))$. This metric is defined such that the NN’s performance is *verified* if $f(x) \geq 0$, $\forall x \in \mathcal{C}$, can be proved:

$$\gamma \triangleq \min_{x \in \mathcal{C}} f(x). \quad (1)$$

In this NN, $\hat{x}^{(i)} = W^{(i)}x^{(i)} + b^{(i)}$ is the i^{th} layer linear transformation, with $x^{(1)} = x$ as the input, and $x^{(i+1)} = \sigma(\hat{x}^{(i)})$ is the associated nonlinear activation. In this paper, $\sigma(\cdot)$ exclusively represents the sigmoid activation function:

$$\sigma(x) \triangleq \frac{e^x}{1 + e^x} = \frac{1}{1 + e^{-x}}, \quad (2)$$

where the gradient of the sigmoid is $\sigma' = \sigma(1 - \sigma)$. As in (Wang et al. 2021), the region \mathcal{C} can be described as an ℓ_p norm ball constraint on the input via $\mathcal{C} = \{x \mid \|x - x_0\|_p \leq \epsilon\}$. To solve (1) to global optimality (or, at least, to prove

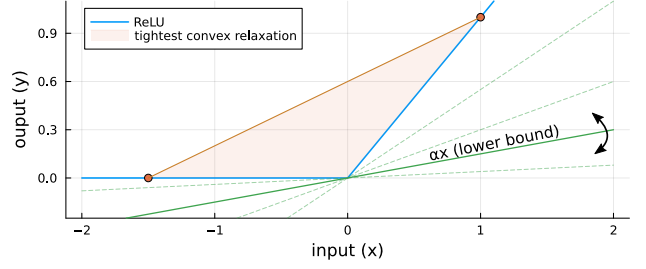


Figure 1: Convex relaxation of ReLU activation function, lower bounded by $y = \alpha x$, with tunable $\alpha \in [0, 1]$.

$\gamma \geq 0$), many recent approaches have utilized (i) convex relaxation of activation functions coupled with (ii) spatial (Shi et al. 2024) and discrete (Wang et al. 2021) Branch-and-Bound (B&B) strategies. B&B iteratively toggles activation function statuses, yielding tighter and tighter solutions, in pursuit of the problem’s true lower bound. In this paper, we exclusively consider the so-called root node relaxation of (1), i.e., the first, and generally loosest, B&B relaxation, where all activation functions are simultaneously relaxed. We denote the root node relaxation of $f(x)$ as $\tilde{f}_r(x)$, where

$$\min_{x \in \mathcal{C}} f(x) \geq \min_{x \in \mathcal{C}} \tilde{f}_r(x). \quad (3)$$

is guaranteed, assuming valid relaxations are applied. While $\tilde{f}_r(x)$ is an easier problem to solve, (Salman et al. 2020) showed that verification over relaxed NNs can face a “convex relaxation barrier” problem; essentially, even tight relaxations are sometimes not strong enough to yield conclusive verification results. In this paper, we seek to find the tightest possible relaxation of the sigmoid activation function.

Sigmoid Activation Function Relaxation

In order to convexly bound the $\text{ReLU}(x) = \max(x, 0)$ activation function, (Xu et al. 2021) famously replaced the tight “triangle” LP-relaxation of an unstable neuron with a tunable lower bound, α , as illustrated in Fig. 1. This α was then iteratively maximized over in the dual space to achieve the tightest lower bound of the relaxed NN. At each gradient step, the value of α was feasibly clipped to $0 \leq \alpha \leq 1$, such that $\alpha x \leq \text{ReLU}(x)$ was always maintained.

In the same spirit, we seek to bound the sigmoid activation function $\sigma(x)$ with tunable affine expressions via

$$\alpha_l x + \beta_l \leq \sigma(x) \leq \alpha_u x + \beta_u, \quad (4)$$

where α_l , β_l , α_u , and β_u are maximized over in the dual space to find the tightest lower bound on the NN relaxation. Analogous to the $0 \leq \alpha \leq 1$ bound from (Xu et al. 2021), however, we must ensure that the numerical values of α_l , β_l , and α_u , β_u always correspond to, respectively, valid lower and upper bounds on the sigmoid activation function.

Definition 1. In this paper,

- $\alpha_l x + \beta_l$ is called an “**affine lower bound**”, while
- $\alpha_u x + \beta_u$ is called an “**affine upper bound**”.

In order to derive the slope α and intercept β terms which yield maximally tight convex relaxation of the sigmoid function, we consider the point at which the associated rotating bound $\alpha x + \beta$ intersects with the sigmoid at some tangent point (the upper u and lower l subscripts are dropped for notational convenience). We encode the intersection (5a) and tangent (5b) point relations via

$$\alpha x + \beta = \sigma(x) \quad (5a)$$

$$\alpha = \sigma'(x), \quad (5b)$$

where $\sigma'(x)$ is the gradient of the sigmoid. The system of (5) represents two equations and three unknowns. In order to maximize over the α and β variables independent of the primal variable x , it is advantageous to eliminate x entirely. Interestingly, the solution for β , written strictly in terms of α , has a closed form solution $\beta = h(\alpha)$ (see appendix for derivation). This solution represents a main result from this paper, and it is given by

$$\beta = \frac{1}{1 + e^{\pm \cosh^{-1}\left(\frac{1}{2\alpha} - 1\right)}} \pm \alpha \cosh^{-1}\left(\frac{1}{2\alpha} - 1\right). \quad (6)$$

In (6), the \pm terms are negative for the upper bounds, and positive for the lower bounds, as stated in the appendix. Associated affine bounds are plotted in Fig. 2. As depicted, these bounds are capable of yielding the tightest possible convex relaxation of the sigmoid activation function. Denoting (6) by $\beta = h(\alpha)$, we define a set \mathcal{S} of valid α, β values:

$$\mathcal{S} = \{\alpha, \beta \mid \beta = h(\alpha), \underline{\alpha} \leq \alpha \leq \bar{\alpha}\}. \quad (7)$$

The minimum and maximum allowable slope values, $\underline{\alpha}$ and $\bar{\alpha}$, are predetermined for every sigmoid activation function. Nominally, $\underline{\alpha} \geq 0$, since $\inf(\sigma'(x)) = 0$, and $\bar{\alpha} \leq 1/4$, since $\sup(\sigma'(x)) = 0.25$. However, tighter slopes generally exist, based on the sigmoid's minimum and maximum input bounds \underline{x} and \bar{x} . Fig. 3 illustrates a typical situation, where there are distinct slope bounds. In this figure, the minimum slopes (dashed lines) are simply computed as the gradients at the minimum and maximum inputs:

$$\underline{\alpha}_l = \sigma'(\underline{x}) \quad (8)$$

$$\underline{\alpha}_u = \sigma'(\bar{x}). \quad (9)$$

The maximum bounding slopes $\bar{\alpha}_l$ and $\bar{\alpha}_u$, however, are computed as the lines which intersect the sigmoid at two points: the bounded input anchor points (\underline{x} and \bar{x}), and a corresponding tangent point. The parallelized calculation of these slopes is a pre-processing step involving sequential quadratic formulate iterations, and the associated procedures are discussed in the appendix.

Fig. 4 illustrates an alternative situation, where the maximum and minimum affine upper bound slopes are equal¹: $\bar{\alpha}_u = \underline{\alpha}_u$. This occurs when the tangent slope at \bar{x} can be

¹ Depending on the values of \underline{x} and \bar{x} , this can also happen to the affine lower bounds: $\bar{\alpha}_l = \underline{\alpha}_l$. However, due to the nonlinearity of the sigmoid, $\bar{\alpha}_l = \underline{\alpha}_l$ and $\bar{\alpha}_u = \underline{\alpha}_u$ cannot occur simultaneously, unless $\bar{x} = \underline{x}$, which is a degenerate case.

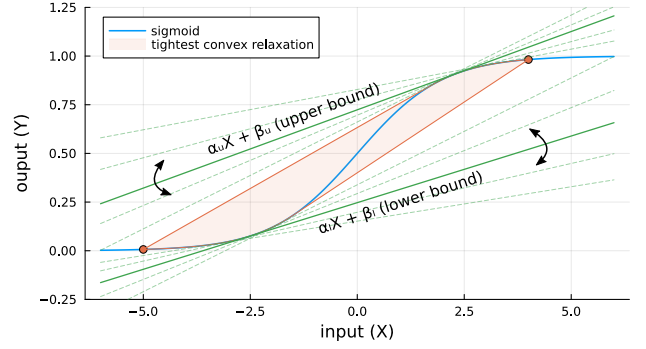


Figure 2: Rotating affine bounds around the sigmoid activation function, achieving maximally tight convex relaxation.

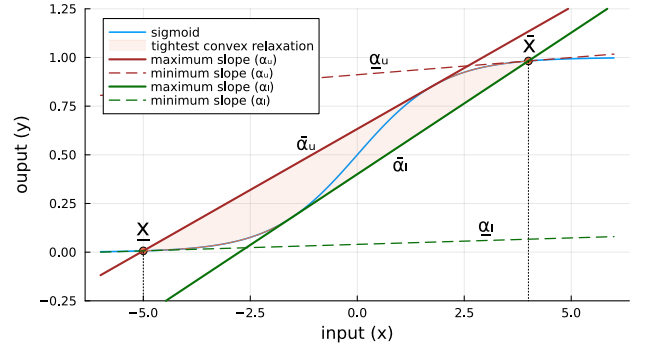


Figure 3: For max and min input values (\bar{x} , \underline{x}), depicted are the steepest and shallowest upper bound slopes ($\bar{\alpha}_u$, $\underline{\alpha}_u$), and the steepest and shallowest lower bound slopes ($\bar{\alpha}_l$, $\underline{\alpha}_l$).

“raised up” such that the corresponding affine bound eventually intersects with \underline{x} . Defining $\Delta x = \bar{x} - \underline{x}$, we have two possibilities:

$$\text{if } \bar{x} - \sigma'(\bar{x})\Delta x \leq \underline{x}, \text{ then } \bar{\alpha}_u = \underline{\alpha}_u \quad (10a)$$

$$\text{if } \bar{x} - \sigma'(\bar{x})\Delta x > \underline{x}, \text{ then } \bar{\alpha}_u > \underline{\alpha}_u. \quad (10b)$$

Similarly, in the lower affine bound case,

$$\text{if } \underline{x} + \sigma'(\underline{x})\Delta x \geq \bar{x}, \text{ then } \bar{\alpha}_l = \underline{\alpha}_l \quad (11a)$$

$$\text{if } \underline{x} + \sigma'(\underline{x})\Delta x < \bar{x}, \text{ then } \bar{\alpha}_l > \underline{\alpha}_l. \quad (11b)$$

In either case, equal slopes can be directly computed as

$$\underline{\alpha}_u = \bar{\alpha}_l = \frac{\sigma(\bar{x}) - \sigma(\underline{x})}{\bar{x} - \underline{x}}. \quad (12)$$

Backward Bound Propagation

To efficiently minimize $\tilde{f}_r(x)$, as in (3), we utilize the backward bound propagation procedure employed in, e.g., (Wang et al. 2021). In applying this procedure, however, we utilize a sequential backward evaluation step in order to dynamically detect if a sigmoid function should be upper, or lower, bounded by the affine bound in (6). Consider, for example, the simple problem

$$\min_{x \in \mathcal{C}} c^T \sigma(x) \geq \min_{x \in \mathcal{C}} c^T (\alpha x + \beta), \quad (13)$$

where c is some cost vector. To achieve minimum cost,

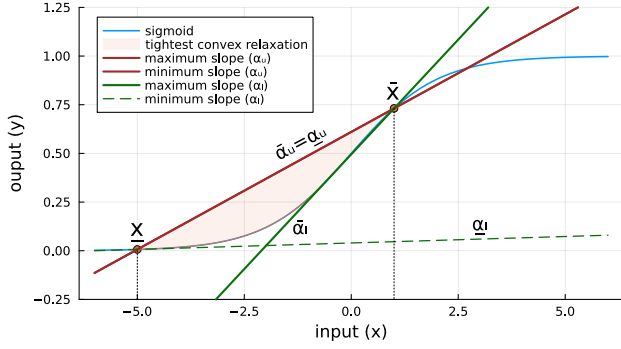


Figure 4: Since the slope at \bar{x} is sufficiently steep, (10a) is applied, and the tightest upper bound is a static line.

- if $c_i \geq 0$, then $\alpha_l x + \beta_l$ should lower bound the sigmoid;
- if $c_i \leq 0$, then $\alpha_u x + \beta_u$ should upper bound the sigmoid.

This procedure is sequentially applied as we move backward through the NN layers. The coefficients in front of each layer, however, will be a function of the numerical α values, which will be changing at each gradient step during the verification solve. In the appendix, we define a NN mapping (20), and then we sequentially move backward through this mapping in (21), inferring the sign of the coefficients in front of each affine bound term.

Dual Verification

Using the affine relaxed version of the NN mapping in (20), we may start with input x to sequentially replace all intermediate primal variables:

$$\tilde{f}_r(x) = c^T(\dots d(\alpha^{(i)})(W^{(i)}(\dots x \dots) + b^{(i)}) + \beta^{(i)} \dots) \quad (14a)$$

$$\triangleq g_1(\alpha, \beta)^T x + g_2(\alpha, \beta). \quad (14b)$$

The associated minimization problem over this relaxed verification problem is given by

$$\min_{x \in \mathcal{C}} \tilde{f}_r(x) = \min_{\|x\|_p \leq \epsilon} g_1(\alpha, \beta)^T x + g_2(\alpha, \beta) \quad (15a)$$

$$= - \underbrace{\|g_1(\alpha, \beta)^T\|_q}_{\tilde{f}_r(\alpha, \beta)} + g_2(\alpha, \beta), \quad (15b)$$

where the dual norm (Wang et al. 2021; Chevalier, Murzakhanov, and Chatzivasileiadis 2024) has been used to transform the p norm constraint into a q norm objective term. Any valid (i.e., feasible) set of α, β parameters will yield a valid lower bound for the relaxed verification problem. To achieve the *tightest* lower bound, we may maximize $\tilde{f}_r(\alpha, \beta)$ over the feasible set \mathcal{S} of α, β :

$$\tilde{\gamma} = \max_{\{\alpha, \beta\} \in \mathcal{S}} - \|g_1(\alpha, \beta)^T\|_q + g_2(\alpha, \beta). \quad (16)$$

While α, β are not dual variables in the traditional sense, they are responsible for actively constraining the primal space, so we refer to (16) as a dual problem.

While (16) can be solved via projected gradient ascent, we may alternatively use $\beta = h(\alpha)$ in order to eliminate the

Algorithm 1: Verifying sigmoid-based NNs with “ α -sig”

Input: \bar{x}, \underline{x} for each activation function

Output: $\tilde{\gamma}$: solution to (17)

- 1: For all sigmoids, parallel compute $\underline{\alpha}$ and $\bar{\alpha}$
- 2: Initialize: $t = \infty$
- 3: **while** $|\tilde{f}_r(\alpha, h(\alpha)) - t| \geq \epsilon$ **do**
- 4: Compute $t = \tilde{f}_r(\alpha, h(\alpha))$
- 5: **for** NN Layers $i = L, L-1, \dots, 1$, **do**
- 6: Compute layer sign vector $s^{(i)}$ in (21)
- 7: Embed $s^{(i)}$ inside of β via (18)
- 8: **end for**
- 9: Back-propagate objective \tilde{f}_r of (17) w.r.t. α
- 10: Take a gradient ascent step with, e.g., Adam
- 11: Clip all α values between $\underline{\alpha}$ and $\bar{\alpha}$
- 12: **end while**
- 13: **return** tight lower bound $\tilde{\gamma} = \tilde{f}_r(\alpha, \beta)$

β variable entirely. Initial testing shows that eliminating β , and then backpropagating through $h(\alpha)$, is more effective than equality projecting feasible, via (6), at each step. The updated formulation is given via

$$\tilde{\gamma} = \max_{\alpha \leq \alpha \leq \bar{\alpha}} - \|g_1(\alpha, h(\alpha))^T\|_q + g_2(\alpha, h(\alpha)). \quad (17)$$

Projected gradient-based solution routine

We use a projected gradient routine in order to solve (17) and enforce $\alpha \leq \alpha \leq \bar{\alpha}$. Sigmoid functions may need to be upper bounded via (29), and then lower bounded via (30), as numerical values of α evolve. To overcome this challenge, at each step of our numerical routine, we reverse propagate compute the sign vector $s^{(i)}$, from (21), for each layer. Since this vector tells us if the sigmoid function should be upper or lower bounded, we embed corresponding elements of this vector inside of (6), replacing the \pm terms. At the j^{th} activation function of each i^{th} NN layer, the corresponding slope and sign elements are feasibly related via

$$\beta_j^{(i)} = \frac{1}{1 + \exp\left(s_j^{(i)} \cosh^{-1}\left(\frac{1}{2\alpha_j^{(i)}} - 1\right)\right)} + s_j^{(i)} \alpha_j^{(i)} \cosh^{-1}\left(\frac{1}{2\alpha_j^{(i)}} - 1\right), s_j^{(i)} \in \pm 1. \quad (18)$$

With this parameterization embedded inside of (17), we backpropagate through the objective function and take a gradient step with α . Next, we clip all values of α to remain between $\underline{\alpha}$ and $\bar{\alpha}$, depending on whether the corresponding α is acting like an upper or lower affine bound. The full gradient-based verification routine for a sigmoid-based NN is given in Alg 1, which we refer to as α -sig. The bounds \bar{x}, \underline{x} for each activation function are treated as inputs.

Test Results

In order to test the effectiveness of α -sig and Alg. 1, we optimized over a range of randomly generated sigmoid-based NNs in two separate experiments. All NNs consisted of four dense layers with sigmoid activation functions, followed by

a dense linear layer. We considered NNs containing 5, 10, 50, 100, 500, and 1000 neurons per layer. For each NN size, we generated and verified over 5 independent NN instantiations. The posed verification problem sought to minimize the sum of all outputs (i.e., the c vector from (20a) was set to the vector of all ones), and we assumed an allowable infinity norm perturbation of $\|x\|_\infty \leq 1$ (i.e., $-1 \leq x \leq 1$). To generate initial loose activation function bounds for all NN layers, we applied vanilla interval bound propagation via (39), as reviewed in the appendix. We note that tighter bounds could potentially be achieved via IBP + backward mode LiRPA (Xu et al. 2020), but we chose to utilize weaker IBP-based bounds to initialize α -sig in order to highlight its effectiveness without strong initial activation function bounds.

In each test, we took 300 projected gradient steps in pursuit of solving (17). We then benchmarked our results against α -CROWN + auto-LiRPA (Xu et al. 2021, 2020). In order to fairly compare, we increased the default α -CROWN iteration count by 3-fold, to 300 iterations. To avoid an early exit from CROWN (i.e., due to a successfully proved bound), we set the VNN-LIB (Ferrari et al. 2022) verification metric to an arbitrarily high value Γ (i.e., prove $f(x) \geq \Gamma, \forall x$). In order to compare the bounds proved via our α -sig in Alg. 1 vs α -CROWN, we defined τ :

$$\tau = 100 \times \frac{\tilde{\gamma} - \text{CROWN}_{\text{bound}}}{|\text{CROWN}_{\text{bound}}|}, \quad (19)$$

where τ represents the percent improvement or decline of our bound relative to α -CROWN (positive τ means α -sig provides a *tighter* bound than α -CROWN, while negative τ means the bound is *looser*). α -sig was built in Julia, and all code is provided as supplementary material.

Experiment 1: Varying weight distributions. Normally distributed weight and bias parameters tend to yield NNs whose sigmoid activation functions are always stuck on or off. In order to avoid this, we initialized all NN weights and biases via $W_i \sim \mathcal{N}(0, (2.5/j)^2)$ and $b_i \sim \mathcal{N}(0, 0.25^2)$, where $j \in \{1, 2, 3, 4, 5\}$ represents the model index; thus, in this experiment, the weight parameter variances for each NN model progressively shrank (for a given model size). Results associated with this test are given in Table 1: in this table, the values τ_1 through τ_5 represent bound comparisons, à la (19), across five independently generated models (five for each NN size). Clearly, α -sig tended to provide marginally tighter bounds than α -CROWN. Across all six NN sizes, the bound progressions for α -sig are illustrated in Fig. 5. In this figure, initial CROWN and fully optimized α -CROWN bounds are superimposed for reference.

In the upper-right portion of Table 1, α -CROWN outperformed α -sig. The reason why is apparent and interesting: in our experiments, α -sig was initialized with fairly loose IBP-based primal bounds \bar{x}, \underline{x} (see input to Alg. 1). As NN models shrink in size and weight parameter variances drop, auto-LiRPA’s proclivity for primal bound solving seems to overtake α -sig’s optimal tightening of the sigmoid activation function. The benefit of α -sig, however, is also in its speed. As demonstrated in Table 2, α -sig can be up to two orders of magnitude faster² than α -CROWN, while still yielding

²One of the trial times was removed due to CROWN error:

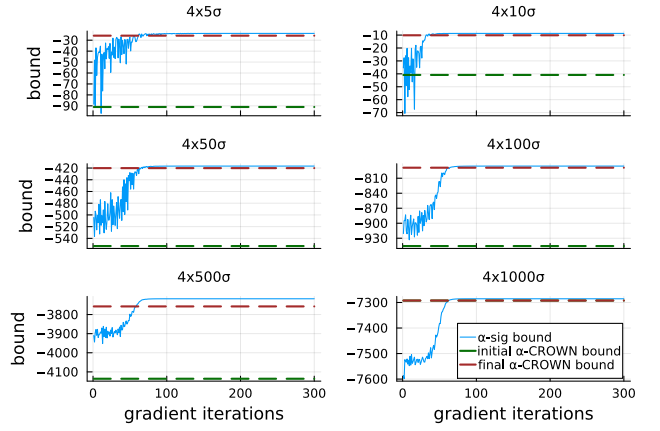


Figure 5: Gradient ascent iterations of α -sig across 6 NN model sizes. Test are associated with τ_1 from Table 1. Initial and final (i.e., optimized) CROWN bounds are also shown.

Table 1: Comparison of α -sig vs α -CROWN bounds (NN weight distribution variance shrink from $\tau_1 \rightarrow \tau_5$).

NN Size	τ_1	τ_2	τ_3	τ_4	τ_5
$4 \times 5\sigma$	+8.02	-18.9	-6.1	-21.2	-31.8
$4 \times 10\sigma$	+14.6	-7.23	-28.1	-26.4	-24.0
$4 \times 50\sigma$	+0.83	+0.51	+0.23	-4.25	-9.63
$4 \times 100\sigma$	+0.40	+0.34	+0.04	-0.52	-1.60
$4 \times 500\sigma$	+1.06	+0.13	+0.14	+0.10	+0.03
$4 \times 1000\sigma$	+0.09	+0.81	+0.11	+0.11	+0.06

better bounds in many cases.

Experiment 2: Consistent weight distributions. In this test, we initialized all NN weights and biases with consistent distributions: $W_i \sim \mathcal{N}(0, 2.5^2)$ and $b_i \sim \mathcal{N}(0, 0.25^2)$. Results from across five randomly initialized models are shown in Table 3. In contrast to the first experiment, α -sig was able to reliably outperform α -CROWN. In this case, the larger weight parameter variances seemed to cause inherently looser primal bounds, meaning α -CROWN’s advantage over α -sig was lessened.

Discussion and Conclusion

Verifying over NNs containing S-shaped activation functions is inherently challenging. In this paper, we presented an explicit, differentiable mapping between the slope and y-intercept of an affine expression which tangentially bounds a sigmoid function. By optimizing over this bound’s parameters in the dual space, our proposed convex relaxation of the sigmoid is maximally tight (i.e., a tighter element-wise relaxation of the sigmoid activation function does not exist). As explored in the test results section, however, our ability to fully exploit this tightness hinges on having good primal bounds \bar{x}, \underline{x} for all activation functions. For example, given

“Pre-activation bounds are too loose for BoundSigmoid”.

Table 2: Mean α -CROWN and α -sig solve times.

NN Size	α -CROWN	α -sig	α -sig speedup
$4 \times 5\sigma$	37.41 sec	0.10 sec	360.4x
$4 \times 10\sigma$	37.77 sec	0.105 sec	358.4x
$4 \times 50\sigma$	38.33 sec	0.17 sec	223.1x
$4 \times 100\sigma$	37.90 sec	0.40 sec	95.1x
$4 \times 500\sigma$	53.42 sec	2.65 sec	20.2x
$4 \times 1000\sigma$	82.90 sec	9.98 sec	8.3x

Table 3: Comparison of α -sig vs α -CROWN bounds (consistent distributions across models 1 through 5).

NN Size	τ_1	τ_2	τ_3	τ_4	τ_5
$4 \times 5\sigma$	-7.30	+17.9	-32.99	-8.12	-0.37
$4 \times 10\sigma$	+4.6	+28.1	-1.31	+2.29	-2.66
$4 \times 50\sigma$	+1.26	+0.49	+0.64	+1.21	+0.95
$4 \times 100\sigma$	+0.47	+0.51	+0.65	+0.70	+0.57
$4 \times 500\sigma$	+0.99	+0.98	+1.02	+0.97	+0.98
$4 \times 1000\sigma$	+0.13	+0.19	+0.09	+0.12	+0.12

the bounds $\bar{x} = \infty$, $\underline{x} = -\infty$, our approach collapses to a useless box constraint.

Even with relatively loose IBP-based activation function bounds, however, our proposed verification routine “ α -sig” is able to (i) marginally outperform α -CROWN in terms of bound tightness, and (ii) substantially outperform it in terms of computational efficiency. Future work will attempt to marry LiRPA/CROWN’s excellent proclivity for activation function bounding with α -sig’s element-wise activation function tightening prowess. Future work will also extend the approach presented in this paper to other S-shaped activation functions, along with the multi-variate softmax function.

APPENDICES

Neural Network Mapping and Relaxation

The NN mapping, whose output is transformed by a verification metric c^T , is stated below. At each sigmoid activation function, we also state the corresponding affine relaxation, where $d(\alpha)$ diagonalizes an α vector into a diagonal matrix:

$$c^T \text{NN}(x) = c^T (W^{(L)} x^{(L)} + b^{(L)}) \quad (20a)$$

$$x^{(L)} = \sigma(\hat{x}^{(L-1)}) : d(\alpha^{(L-1)}) \hat{x}^{(L-1)} + \beta^{(L-1)} \quad (20b)$$

$$\hat{x}^{(L-1)} = W^{(L-1)} x^{(L-1)} + b^{(L-1)} \quad (20c)$$

$$\vdots$$

$$x^{(3)} = \sigma(\hat{x}^{(2)}) : d(\alpha^{(2)}) \hat{x}^{(2)} + \beta^{(2)} \quad (20d)$$

$$\hat{x}^{(2)} = W^{(2)} x^{(2)} + b^{(2)} \quad (20e)$$

$$x^{(2)} = \sigma(\hat{x}^{(1)}) : d(\alpha^{(1)}) \hat{x}^{(1)} + \beta^{(1)} \quad (20f)$$

$$\hat{x}^{(1)} = W^{(1)} x^{(1)} + b^{(1)} \quad (20g)$$

$$x^{(1)} = x. \quad (20h)$$

We may now relax the sigmoid activation functions, replacing them with their affine bounds. To determine if each scalar α , β pair are chosen to be an upper bound or a lower bound, we need to determine the coefficient in front of the corresponding activation function. To do this, we move backward through the NN, defining vectors $s^{(i)}$ of sign values corresponding to the signs of the entries in the argument:

$$s^{(L)} = \text{sign}(c^T W^{(L)}) \quad (21a)$$

$$s^{(L-1)} = \text{sign}(c^T W^{(L)} d(\alpha^{(L-1)}) W^{(L-1)}) \quad (21b)$$

$$\vdots$$

$$s^{(2)} = \text{sign}(c^T W^{(L)} d(\alpha^{(L-1)}) W^{(L-1)} \dots d(\alpha^{(2)}) W^{(2)}) \quad (21c)$$

$$s^{(1)} = \text{sign}(c^T W^{(L)} d(\alpha^{(L-1)}) W^{(L-1)} \dots d(\alpha^{(2)}) W^{(2)} d(\alpha^{(1)}) W^{(1)}) \quad (21d)$$

Slope and Intercept Relation Derivation

Starting from (5b), the sigmoid derivative can be written via $\sigma'(x) = \sigma(x)(1 - \sigma(x))$. Setting this equal to the upper affine bound slope, we have

$$\alpha = \frac{1}{1 + e^{-x}} \left(1 - \frac{1}{1 + e^{-x}} \right) \quad (22a)$$

$$= \frac{e^{-x}}{(1 + e^{-x})^2}. \quad (22b)$$

Multiplying through by the expanded right-side denominator, we may solve for the primal variable x explicitly:

$$\alpha (1 + e^{-2x} + 2e^{-x}) = e^{-x} \quad (23)$$

$$\alpha (e^x + e^{-x} + 2) = 1 \quad (24)$$

$$2\alpha (\cosh(x) + 1) = 1 \quad (25)$$

$$x = \pm \cosh^{-1} \left(\frac{1}{2\alpha} - 1 \right). \quad (26)$$

Since $\cosh(x) = \cosh(-x)$, the solution for x is non-unique, which is an inherent consequence of the symmetry of the sigmoid function, where exactly two points in the sigmoid manifold will map to the same slope. Notably, however, the affine upper bound will map to positive solutions

of x , i.e., in the region where the sigmoid function is concave, and the affine lower bound will map to negative values of x , i.e., in the region where the sigmoid function is convex:

$$x = \cosh^{-1} \left(\frac{1}{2\alpha_u} - 1 \right) \quad (27)$$

$$x = -\cosh^{-1} \left(\frac{1}{2\alpha_l} - 1 \right). \quad (28)$$

Reorganizing the intersection equation (5a), such that $\beta = 1/(1 + e^{-x}) - \alpha x$, we may plug the primal solutions (27)-(28) in for x . This yields explicit expressions for the intercept points (β_u, β_l) as functions of the slopes (α_u, α_l) :

$$\beta_u = \frac{1}{1 + e^{-\cosh^{-1}(\frac{1}{2\alpha_u} - 1)}} - \alpha \cosh^{-1} \left(\frac{1}{2\alpha_u} - 1 \right) \quad (29)$$

$$\beta_l = \frac{1}{1 + e^{+\cosh^{-1}(\frac{1}{2\alpha_l} - 1)}} + \alpha \cosh^{-1} \left(\frac{1}{2\alpha_l} - 1 \right). \quad (30)$$

Computing Maximum Slope Limits

In order to compute the maximum slope values $\bar{\alpha}_l$ and $\bar{\alpha}_u$, as depicted in Fig. 3, we use a sequential numerical routine which iteratively solves a quadratic expansion of the associated problem. Consider the following system of equations, with unknown variables α , β , and \hat{x} (intercept point):

$$\underline{y} = \alpha \underline{x} + \beta \quad \text{anchor point} \quad (31)$$

$$\sigma(\hat{x}) = \alpha \hat{x} + \beta \quad \text{sigmoid intersection at } \hat{x} \quad (32)$$

$$\sigma(\hat{x})' = \alpha \quad \text{match sigmoid slope at } \hat{x}, \quad (33)$$

where the known ‘‘anchor point’’ $(\underline{x}, \underline{y})$ is depicted in Fig. 6. Despite its similarity to (5), this system does not have a closed-form solution (i.e., it will result in a single nonlinear equation, similar to (6), but with β replaced by an expression for α). In order to efficiently solve this system of equations, we perform a single quadratic expansion of the sigmoid activation function (Agarwal et al. 2022):

$$\sigma(\hat{x}) \approx \tilde{\sigma}(\hat{x}) \triangleq \sigma_0 + \sigma'_0(\hat{x} - \hat{x}_0) + \frac{1}{2}\sigma''_0(\hat{x} - \hat{x}_0)^2, \quad (34)$$

where $\sigma_0 \triangleq \sigma(x)|_{\hat{x}_0}$, etc., is used for notational simplicity. Collecting like powers of \hat{x} , the quadratic expansion yields

$$\begin{aligned} \tilde{\sigma}(\hat{x}) &= \sigma_0 + \sigma'_0\hat{x} - \sigma'_0\hat{x}_0 + \frac{1}{2}\sigma''_0(\hat{x}^2 + \hat{x}_0^2 - 2\hat{x}\hat{x}_0) \\ &= \sigma_0 + \sigma'_0\hat{x} - \sigma'_0\hat{x}_0 + \frac{1}{2}\sigma''_0\hat{x}^2 + \frac{1}{2}\sigma''_0\hat{x}_0^2 - \sigma''_0\hat{x}\hat{x}_0 \\ &= \underbrace{\left(\sigma_0 - \sigma'_0\hat{x}_0 + \frac{1}{2}\sigma''_0\hat{x}_0^2\right)}_{c_0} + \underbrace{(\sigma'_0 - \sigma''_0\hat{x}_0)}_{c_1}\hat{x} + \underbrace{\frac{1}{2}\sigma''_0}_{c_2}\hat{x}^2. \end{aligned}$$

The updated system of equations is now quadratic:

$$\underline{y} = \alpha \underline{x} + \beta \quad \text{anchor point} \quad (35)$$

$$c_2\hat{x}^2 + c_1\hat{x} + c_0 = \alpha \hat{x} + \beta \quad \text{approx intersection} \quad (36)$$

$$2c_2\hat{x} + c_1 = \alpha \quad \text{approx slope match.} \quad (37)$$

In this system, we may eliminate the α and β terms by setting $\alpha = 2c_2\hat{x} + c_1$ and $\beta = \underline{y} - \alpha\underline{x}$, which yields

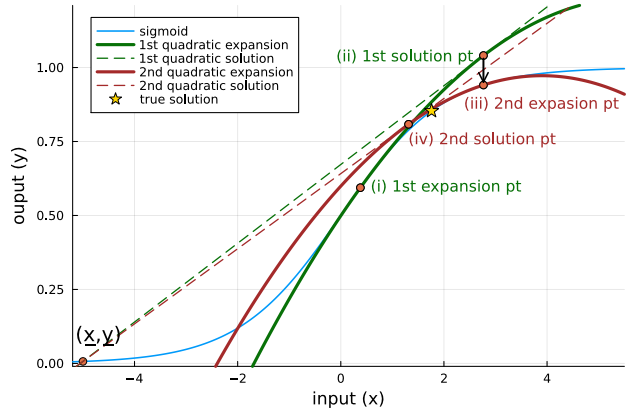


Figure 6: Sequential quadratic expansions and solutions.

$\beta = \underline{y} - (2c_2\hat{x} + c_1)\underline{x}$. Plugging these into (36), a single quadratic equation emerges:

$$c_2\hat{x}^2 + c_1\hat{x} + c_0 = (2c_2\hat{x} + c_1)\hat{x} + \underline{y} - (2c_2\hat{x} + c_1)\underline{x}.$$

We reorganize these terms into a standard quadratic form:

$$0 = \underbrace{(c_2)}_{d_2(\hat{x}_0)}\hat{x}^2 + \underbrace{(-2c_2\underline{x})}_{d_1(\hat{x}_0)}\hat{x} + \underbrace{(\underline{y} - c_1\underline{x} - c_0)}_{d_0(\hat{x}_0)}, \quad (38)$$

where coefficients d_2, d_1, d_0 are written as functions of the expansion point \hat{x}_0 . We use the quadratic formula to analytically solve (38). Multiple iterations of (i) updating the d coefficients and then (ii) re-solving (38) via quadratic formula yields rapidly converging solutions to the original system (31)-(33). Due to the analytical exactness of the quadratic formula, this routine converges faster than Newton iterations at a similar computational expense. Two iterations of this routine are depicted in Fig. 6, where the second solution falls very close to the true solution (which future iterations converge to). Once the solution \hat{x}^* is found, we recover α via $\alpha = \sigma'(\hat{x}^*)$. The procedure is applied to find the maximum upper affine bound slope in Fig. 6; an identical procedure is applied to find the maximum lower affine bound slope.

Interval Bound Propagation

In order to propagate input bounds $\underline{x} \leq x \leq \bar{x}$ through a NN layer $y = \sigma(W_i x + b_i)$, we employ interval bound propagation (Gowal et al. 2019). Defining mean $x_\mu = \frac{1}{2}(\bar{x} + \underline{x})$ and deviation $x_\sigma = \frac{1}{2}(\bar{x} - \underline{x})$ vectors, the output bound vectors are given as

$$\bar{y} = \sigma(|W_i| x_\sigma + W_i x_\mu + b_i) \quad (39a)$$

$$\underline{y} = \sigma(-|W_i| x_\sigma + W_i x_\mu + b_i), \quad (39b)$$

where $\sigma(\cdot)$ can be any element-wise monotonic activation function (Gowal et al. 2019).

Acknowledgments

The authors thank Dr. Amrit Pandey, who suggested the idea of using sequential quadratic expansions of the sigmoid function in order to solve (31)-(33).

References

- Agarwal, A.; Pandey, A.; Bandele, N. T.; and Pileggi, L. 2022. Generalized Smooth Functions for Modeling Steady-State Response of Controls in Transmission and Distribution. *Electric Power Systems Research*, 213: 108657.
- Brix, C.; Bak, S.; Liu, C.; and Johnson, T. T. 2023a. The Fourth International Verification of Neural Networks Competition (VNN-COMP 2023): Summary and Results. arXiv:2312.16760.
- Brix, C.; Müller, M. N.; Bak, S.; Johnson, T. T.; and Liu, C. 2023b. First Three Years of the International Verification of Neural Networks Competition (VNN-COMP). arXiv:2301.05815.
- Bunel, R.; Hinder, O.; Bhojanapalli, S.; Krishnamurthy; and Dvijotham. 2020. An efficient nonconvex reformulation of stagewise convex optimization problems. arXiv:2010.14322.
- Chevalier, S.; and Chatzivasileiadis, S. 2024. Global Performance Guarantees for Neural Network Models of AC Power Flow. arXiv:2211.07125.
- Chevalier, S.; Murzakhanov, I.; and Chatzivasileiadis, S. 2024. GPU-Accelerated Verification of Machine Learning Models for Power Systems. *Hawaii International Conference on System Sciences*.
- Everett, M. 2021. Neural network verification in control. In *2021 60th IEEE Conference on Decision and Control (CDC)*, 6326–6340. IEEE.
- Ferrari, C.; Muller, M. N.; Jovanovic, N.; and Vechev, M. 2022. Complete verification via multi-neuron relaxation guided branch-and-bound. *arXiv preprint arXiv:2205.00263*.
- Gowal, S.; Dvijotham, K.; Stanforth, R.; Bunel, R.; Qin, C.; Uesato, J.; Arandjelovic, R.; Mann, T.; and Kohli, P. 2019. On the Effectiveness of Interval Bound Propagation for Training Verifiably Robust Models. arXiv:1810.12715.
- Henriksen, P.; and Lomuscio, A. 2020. Efficient neural network verification via adaptive refinement and adversarial search. In *ECAI 2020*, 2513–2520. IOS Press.
- Ildiz, M. E.; Huang, Y.; Li, Y.; Rawat, A. S.; and Oymak, S. 2024. From Self-Attention to Markov Models: Unveiling the Dynamics of Generative Transformers. arXiv:2402.13512.
- Lyu, Z.; Ko, C.-Y.; Kong, Z.; Wong, N.; Lin, D.; and Daniel, L. 2019. Fastened CROWN: Tightened Neural Network Robustness Certificates. arXiv:1912.00574.
- Salman, H.; Yang, G.; Zhang, H.; Hsieh, C.-J.; and Zhang, P. 2020. A Convex Relaxation Barrier to Tight Robustness Verification of Neural Networks. arXiv:1902.08722.
- Shi, Z.; Jin, Q.; Kolter, Z.; Jana, S.; Hsieh, C.-J.; and Zhang, H. 2024. Neural Network Verification with Branch-and-Bound for General Nonlinearities. arXiv:2405.21063.
- Singh, G.; Gehr, T.; Püschel, M.; and Vechev, M. 2019. An abstract domain for certifying neural networks. *Proceedings of the ACM on Programming Languages*, 3(POPL): 1–30.
- Sun, L.; Huang, Y.; Wang, H.; Wu, S.; Zhang, Q.; Li, Y.; Gao, C.; Huang, Y.; Lyu, W.; Zhang, Y.; Li, X.; Liu, Z.; Liu, Y.; Wang, Y.; Zhang, Z.; Vidgen, B.; Kailkhura, B.; Xiong, C.; Xiao, C.; Li, C.; Xing, E.; Huang, F.; Liu, H.; Ji, H.; Wang, H.; Zhang, H.; Yao, H.; Kellis, M.; Zitnik, M.; Jiang, M.; Bansal, M.; Zou, J.; Pei, J.; Liu, J.; Gao, J.; Han, J.; Zhao, J.; Tang, J.; Wang, J.; Vanschoren, J.; Mitchell, J.; Shu, K.; Xu, K.; Chang, K.-W.; He, L.; Huang, L.; Backes, M.; Gong, N. Z.; Yu, P. S.; Chen, P.-Y.; Gu, Q.; Xu, R.; Ying, R.; Ji, S.; Jana, S.; Chen, T.; Liu, T.; Zhou, T.; Wang, W.; Li, X.; Zhang, X.; Wang, X.; Xie, X.; Chen, X.; Wang, X.; Liu, Y.; Ye, Y.; Cao, Y.; Chen, Y.; and Zhao, Y. 2024. TrustLLM: Trustworthiness in Large Language Models. arXiv:2401.05561.
- Trinh, T. H.; Wu, Y.; Le, Q. V.; He, H.; and Luong, T. 2024. Solving olympiad geometry without human demonstrations. *Nature*, 625(7995): 476–482.
- Urban, C.; and Miné, A. 2021. A Review of Formal Methods applied to Machine Learning. arXiv:2104.02466.
- Wang, S.; Zhang, H.; Xu, K.; Lin, X.; Jana, S.; Hsieh, C.-J.; and Kolter, J. Z. 2021. Beta-crown: Efficient bound propagation with per-neuron split constraints for neural network robustness verification. *Advances in Neural Information Processing Systems*, 34: 29909–29921.
- Wei, D.; Wu, H.; Wu, M.; Chen, P.-Y.; Barrett, C.; and Farchi, E. 2023. Convex Bounds on the Softmax Function with Applications to Robustness Verification. arXiv:2303.01713.
- Wu, H.; Tagomori, T.; Robey, A.; Yang, F.; Matni, N.; Pappas, G.; Hassani, H.; Pasareanu, C.; and Barrett, C. 2023. Toward Certified Robustness Against Real-World Distribution Shifts. In *2023 IEEE Conference on Secure and Trustworthy Machine Learning (SaTML)*, 537–553.
- Wu, Y.; and Zhang, M. 2021. Tightening Robustness Verification of Convolutional Neural Networks with Fine-Grained Linear Approximation. *Proceedings of the AAAI Conference on Artificial Intelligence*, 35(13): 11674–11681.
- Xu, K.; Shi, Z.; Zhang, H.; Wang, Y.; Chang, K.-W.; Huang, M.; Kailkhura, B.; Lin, X.; and Hsieh, C.-J. 2020. Automatic Perturbation Analysis for Scalable Certified Robustness and Beyond. arXiv:2002.12920.
- Xu, K.; Zhang, H.; Wang, S.; Wang, Y.; Jana, S.; Lin, X.; and Hsieh, C.-J. 2021. Fast and Complete: Enabling Complete Neural Network Verification with Rapid and Massively Parallel Incomplete Verifiers. In *International Conference on Learning Representations*.
- Zhang, H.; Wang, S.; Xu, K.; Wang, Y.; Jana, S.; Hsieh, C.-J.; and Kolter, Z. 2022a. A Branch and Bound Framework for Stronger Adversarial Attacks of ReLU Networks. In Chaudhuri, K.; Jegelka, S.; Song, L.; Szepesvari, C.; Niu, G.; and Sabato, S., eds., *Proceedings of the 39th International Conference on Machine Learning*, volume 162 of *Proceedings of Machine Learning Research*, 26591–26604. PMLR.
- Zhang, Z.; Wu, Y.; Liu, S.; Liu, J.; and Zhang, M. 2022b. Provably Tightest Linear Approximation for Robustness Verification of Sigmoid-like Neural Networks. arXiv:2208.09872.